Journal of Materials Chemistry

Cite this: J. Mater. Chem., 2012, 22, 20026

www.rsc.org/materials

PAPER

Facile conversion of a cellulose acetate laminate film to graphene by a lamination process and post-annealing†

Donghyuk Kim, Ji Yeon Han, Dongchan Lee, Yonghee Lee and Duk Young Jeon*

Received 6th June 2012, Accepted 2nd August 2012
DOI: 10.1039/c2jm33653g

We have demonstrated a simple method for the synthesis of large area and mono- to few-layer graphene on a nickel foil. A cellulose acetate laminate film was coated on a nickel foil as a solid carbon source. Compared to previous synthesis methods using solid carbon sources, the mentioned carbon source can be easily coated on the metal catalyst layer. The uniform graphene layer could be grown on the nickel catalyst layer due to the uniformity of the solid carbon source layer, which was made of a cellulose acetate laminate film coated by the cold press lamination process. The graphene was grown from the cellulose acetate laminate film without explosive gaseous carbon sources usually used in the growth of graphene by CVD methods. A series of processes mentioned above could start and end with the lamination process. In order to control the thickness of the graphene layer, the graphene samples were annealed at various temperatures and durations. The sheet resistance and transmittance of the transferred graphene on a PET substrate were 4240–100 Ω $sq.^{-1}$ and 85–60%, respectively. To demonstrate the practical use of graphene, a flexible PLED was fabricated on the graphene electrode synthesized through the method mentioned above. The maximum luminance and luminance efficiency were 4040 Cd m^{-2} at 6.8 V and 8.2 Cd A^{-1} at 4.0 V. To our knowledge, this is the first report on a typical PLED fabricated on the graphene electrode from a solid carbon source.

Introduction

In recent years, graphene has attracted great interest because of its superb electronic and mechanical properties. Graphene has been considered as a potential candidate for transparent conductive electrodes due to its high transparency and electrical conductivity.[1–12] In order to apply graphene as the transparent conductive electrode, synthesis of large-area, uniform, transparent and conductive graphene is needed. Much research has been carried out for the synthesis of graphene since the graphene was first detached from graphite and transferred onto an arbitrary substrate in 2004.[13] Synthesis of large-area graphene, has been attempted by various methods such as chemical and electrochemical exfoliation,[1–4] chemical vapor deposition (CVD),[5–11] and epitaxial growth.[14,15] Among these methods, the epitaxial growth method has some difficulties such as detaching the graphene from substrates and high cost due to expensive substrates.[16] The chemical exfoliation method has been suggested as a possible approach to scalable synthesis; however, the electrical conductivity of the chemically exfoliated graphene is still lower than that of the graphene grown by CVD.[3] The most advanced synthesis method is CVD using a gaseous hydrocarbon source such as methane or acetylene. The graphene grown by CVD exhibits the highest transmittance and electrical conductivity.[11]

It is also possible to synthesize graphene by annealing other reported carbon sources. Recently, growth of graphene from other carbon sources has been reported. One such reported carbon source is solid carbon such as a highly oriented pyrolytic graphite, amorphous carbon, fullerene, and carbon dissolved or ion implanted into a bulk metal catalyst.[16–23] However, growth of graphene from these solid carbons has limitations that originate from performing vacuum deposition or ion implantation. Another carbon source reported for the synthesis of graphene is a polymer. The polymer can be spin-coated on a metal catalyst layer and subsequently converted to graphene.[24–27] Graphene was grown even from food, insects, and waste.[28] However, these approaches have suggested just a possibility of synthesis of graphene from solid carbon sources.

Our approach for the growth of graphene is using a cellulose acetate laminate film (CALF) as the carbon source. Compared to previous synthesis methods, the large-area carbon source can be easily coated on a metal catalyst layer by a lamination process. A large-area graphene layer can be grown on a metal catalyst layer from a CALF by post-annealing the uniformly coated large-area CALF. Graphene was grown from the CALF without explosive

Department of Materials Science and Engineering, Korea Advanced Institute of Science and Technology, 335 Gwahangno, Yuseong-gu, Daejeon 305-701, Republic of Korea. E-mail: dyj@kaist.ac.kr; Fax: +82-42-350-3310; Tel: +82-42-350-3337

† Electronic supplementary information (ESI) available: Fitted Raman spectra, optical microscope images, comparison of transmittance *versus* sheet resistance for graphene samples from this work with those from gas-source CVD products reported before, Raman D to G peak ratio, 2D to G peak ratio, and FWHM of the 2D peak of graphene annealed under various conditions. See DOI: 10.1039/c2jm33653g

gaseous carbon sources usually used in a CVD method, such as methane. After growth of graphene, the graphene on a nickel foil was transferred onto an arbitrary substrate such as glass or PET film. A series of processes mentioned above could be started and ended with a lamination process. As a practical application, the resulting graphene film was applied to a flexible and solution processable polymer light emitting diode (PLED). The flexible PLED based on the flexible and transparent graphene electrode was fabricated by the solution process, showing the promising possibility of graphene as a flexible and transparent electrode. Our approach of synthesis and transfer of graphene by the lamination process could suggest a significant jump toward the scalable synthesis from solid carbon sources and industrial application of graphene.

Experimental

Synthesis of graphene samples

Graphene was grown by annealing a nickel foil coated with the CALF. A 100 μm thick CALF was coated on a 10 μm thick nickel foil (2×2 cm^2) by using the cold press lamination process and the nickel foil coated with the CALF was inserted into a tube furnace. The samples were annealed at 800 °C, 850 °C, 900 °C and 950 °C, respectively for 10 minutes in an ambient atmosphere with Ar at a flow rate of 700 sccm. After annealing, the samples were rapidly cooled to room temperature by removing the samples from the hot zone to room temperature using a magnetic rod. After growth of graphene, the graphene on nickel foil was transferred onto an arbitrary substrate such as glass or SiO_2 wafer or PET. 5 wt% PMMA dissolved in toluene was spin-coated on the samples at 2000 rpm for 1 minute and subsequently the PMMA coated samples were heated on a hot plate at 180 °C for 1 minute. Then the PMMA/graphene/nickel foil samples were floated over $FeCl_3$ solution to etch the nickel foil. After etching the nickel foil, PMMA/graphene samples were transferred onto an arbitrary substrate such as glass or SiO_2 wafer or PET. Subsequently, the PMMA layer was removed by acetone.[6,9,18] The graphene could be transferred onto a flexible substrate such as PET by the hot press lamination process. To treat the graphene samples with HNO_3, the samples were dipped in a HNO_3 solution for 5 minutes.

Fabrication of a flexible PLED

A PMMA layer was spin-coated on a graphene/nickel foil and subsequently the nickel foil was etched by $FeCl_3$ solution. Then, the synthesized graphene was transferred onto a PET substrate after removing the PMMA layer by acetone. The flexible PLED was fabricated on a graphene/PET substrate by a solution process. The PEDOT:PSS layer was spin-coated on the graphene/PET substrate at 1500 rpm for 60 seconds and subsequently the PEDOT:PSS coated graphene/PET substrate was heated on a hot plate at 140 °C for 30 minutes. For an emissive layer of a PLED, the commercially available polymer, known as "Super Yellow-PPV" (Merck, PDY 132) was dissolved in toluene at a concentration of 4 mg ml^{-1}. On top of the PEDOT:PSS layer, the SY-PPV solution was spin-coated at 2000 rpm for 60 seconds. Finally, a 1 nm thick LiF layer and a 120 nm thick aluminum layer were deposited by thermal evaporation.

Characterization

Raman spectra were obtained using Horiba jobin Yvon (LabRAM HR UV/Vis/NIR at 514 nm). The optical transmittance of prepared samples was measured at the wavelength of 550 nm using a UV-vis spectrometer (Shimadzu UV-3101 PC spectrometer). The sheet resistance of graphene samples was measured by the van der Pauw four probe method. The luminance *vs.* applied voltage characteristics were measured using a Keithley 2400 source measurement unit and a Konica Minolta spectroradiometer (CS-2000).

Results and discussions

Fig. 1 illustrates the procedure for the growth of graphene from the CALF. Graphene was grown by annealing the nickel foil coated with the CALF. The CALF was coated on a nickel foil by the cold press lamination process and the nickel foil coated with the CALF was annealed in an ambient atmosphere with Ar. After annealing, the samples were rapidly cooled to room temperature. During the annealing process, the CALF decomposed into carbon, and the carbon atoms dissolved and diffused into the nickel foil. During the rapid cooling, the dissolved and diffused carbon atoms precipitated from the bulk nickel foil to both sides of the nickel foil. After growth of graphene, the graphene on nickel foil was transferred onto arbitrary substrates such as glass or SiO_2 wafer. The graphene could be transferred onto a flexible substrate such as PET by the hot press lamination process. To treat the graphene samples with HNO_3, the samples were dipped in a HNO_3 solution for 5 minutes.

Raman spectroscopy is a powerful tool to determine the number of graphene layers and the quality of graphene.[29] In order to analyze these properties, Raman spectroscopic analysis (LabRAM HR UV/Vis/NIR at 514 nm, Horiba Jobin Yvon, France) was carried out. Fig. 2 shows the Raman spectra of the graphene grown from the CALF annealed at various temperatures. For all samples, Raman spectra show the typical feature of graphene. Three peaks are observed at ~1350 cm^{-1}, ~1595 cm^{-1}, and ~2700 cm^{-1}, corresponding to the D peak, G peak, and 2D peak, respectively. The shape of the 2D peak, the full width half maximum (FWHM) of the 2D peak, and the intensity ratio of the 2D to G peak are very important to analyze the number of graphene layers. First, the intensity ratio of the 2D to G peak being higher than 2, from 1 to 2, and lower than 1 indicates the monolayer, bilayer, and few layer graphene, respectively. Second, the FWHM of the 2D peak being lower than 45 cm^{-1}, from 45 to 60 cm^{-1}, and higher than 60 cm^{-1} suggests monolayer, bilayer, and a few layer graphene, respectively. Third, the shape of the 2D peak indicates the number of graphene layers. Only the shape of the 2D peak of the monolayer graphene can be fitted with a single Lorentzian curve and is symmetric. The shape of the 2D peak of the bilayer graphene cannot be fitted with a single Lorentzian, but with four Lorentzian curves and is asymmetric. The shape of the 2D peak of the few-layer graphene also cannot be fitted with a single Lorentzian curve and is asymmetric.[30–32] According to these criteria, mono- to few-layer graphene was grown for all samples annealed at 800 °C, 850 °C, 900 °C, and 950 °C, respectively. As shown in Fig. 2a, the intensity ratio of the 2D to G peak of the graphene is

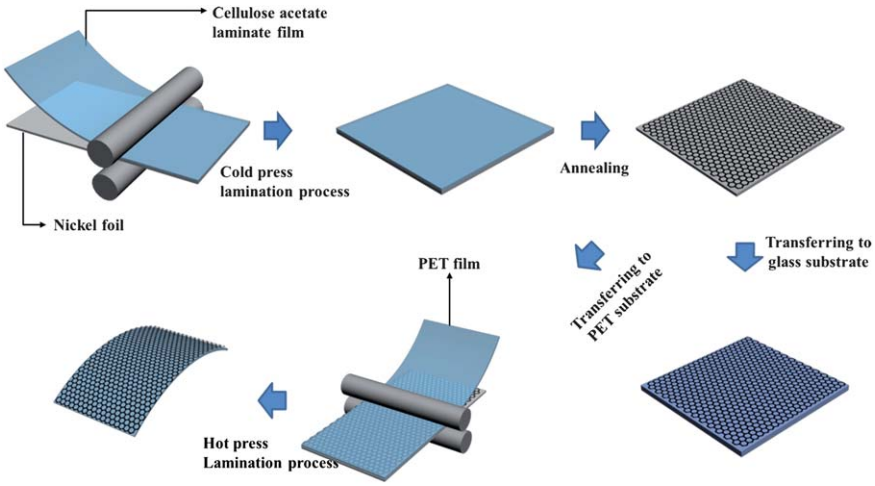

Fig. 1 Schematics of growth of graphene from a CALF. A 10 μm thick nickel foil was coated with the 100 μm thick CALF by the cold press lamination process. After annealing samples in an ambient atmosphere with Ar, graphene was transferred onto a glass or PET substrate. In order to transfer graphene onto the PET substrate, the nickel foil was coated with PET (PET/graphene/nickel foil) by the hot press lamination process and then etched by $FeCl_3$ solution.

higher than 2 and the FWHM is lower than 45 cm^{-1}. In addition, the shape of the 2D peak is well fitted with a single Lorentzian curve and is symmetric (see Table S1 and Fig. S1, ESI†). It indicates that the number of graphene layers is one. In Fig. 2b, the intensity ratio of the 2D to G peak of the graphene is from 1 to 2 and the FWHM is from 45 to 60 cm^{-1}. The shape of the 2D peak is not fitted with a single Lorentzian, but with four Lorentzian curves and is asymmetric (see Fig. S2, ESI†). Fig. 2c shows the Raman spectra of the few-layer graphene. The intensity ratio of the 2D to G peak of the graphene is lower than 1 and the FWHM is higher than 60 cm^{-1}. Fig. 2d shows the intensity ratio of the D to G peak of the samples annealed at various temperatures. The intensity ratio of the D to G peak is an important index to identify the quality of graphene because the D

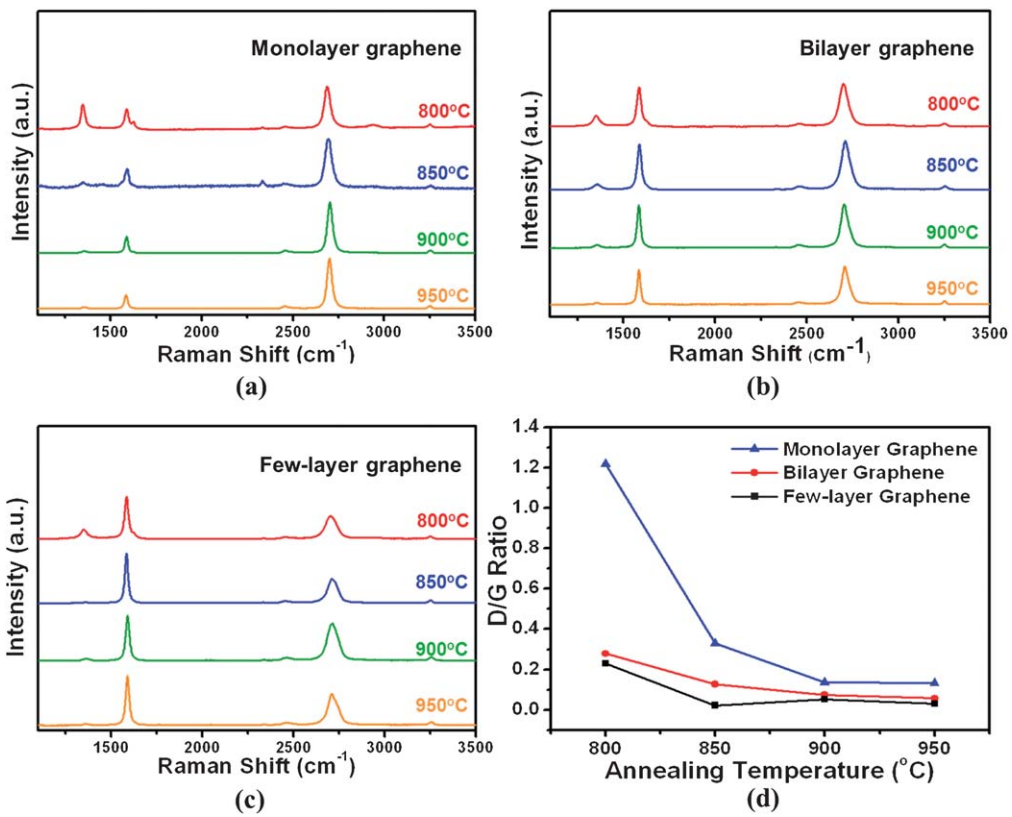

Fig. 2 (a) Raman spectra of monolayer graphene annealed at various temperatures. (b) Raman spectra of bilayer graphene annealed at various temperatures. (c) Raman spectra of few-layer graphene annealed at various temperatures. (d) Ratio of the D to G peak of graphene annealed at various temperatures.

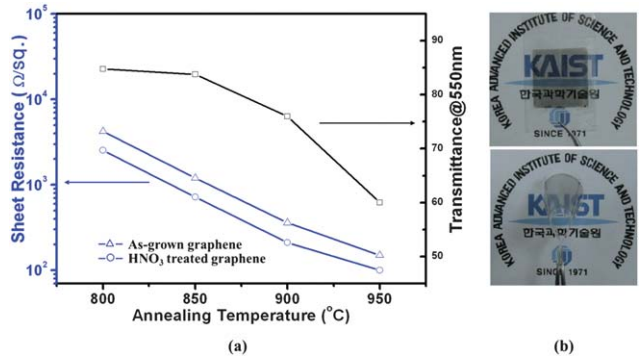

Fig. 3 (a) Sheet resistance and transmittance of graphene annealed at various temperatures. (b) Photo images of graphene on a PET substrate. Graphene was transferred onto the PET substrate by the hot press lamination process. Sheet resistance: 250 Ω sq.$^{-1}$, transmittance: 64%.

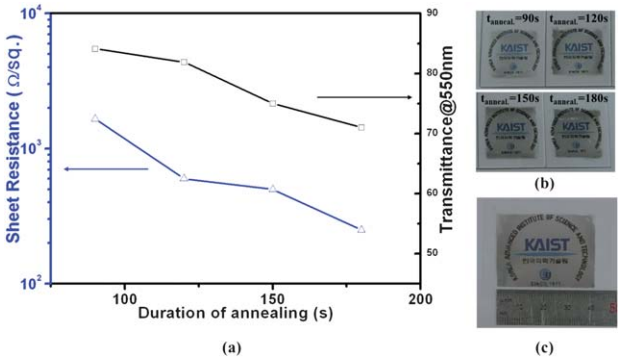

Fig. 5 (a) Sheet resistance and transmittance of graphene annealed for various durations. (b) Photo images of graphene on a glass substrate. (c) Photo image of a 4 × 3 cm^2 graphene on a PET substrate. Sheet resistance: 180 Ω sq.$^{-1}$, transmittance: 63%.

peak originates from defects present in graphene. As shown in Fig. 2d, the intensity ratio of D to G decreased with increasing annealing temperature. With increasing annealing temperature, high quality graphene was grown on the nickel foil.

Fig. 3a shows the sheet resistance and transmittance of the graphene samples annealed at various temperatures and treated with HNO_3. The sheet resistance and transmittance of the as-grown graphene samples were measured after transferring onto a PET substrate. The sheet resistance of as-grown graphene samples were 4240, 1200, 360, and 150 Ω sq.$^{-1}$ at 800, 850, 900, and 950 °C, respectively. The transmittance of as-grown graphene samples at 550 nm were 85, 84, 76, and 60%, respectively. The sheet resistance and the transmittance decreased with increasing annealing temperature. An amount of carbon diffusing into the nickel foil is affected by temperature. The number of carbon atoms that diffuse from the CALF into nickel foil is given by:

$$J_c = -D_c\frac{\partial C_c}{\partial x} \quad \text{atoms} \quad \text{m}^{-2}\ \text{s}^{-1} \tag{1}$$

where D_c is the diffusion coefficient, C_c is the concentration of carbon, and x is the position. This equation is known as Fick's first law of diffusion. The diffusion coefficient is closely related to the temperature. This can be simplified to an Arrhenius-type equation, that is

$$D_c = D_{co}\exp\left(-\frac{Q_{ID}}{RT}\right) \tag{2}$$

where D_{co} is the maximum diffusion coefficient at infinite temperature and Q_{ID} is the activation enthalpy for the diffusion. The diffusion coefficient increases exponentially with temperature.[33] Therefore a higher annealing temperature allows a larger amount of carbon to diffuse into the nickel. Subsequently, a large amount of carbon diffuses and precipitates on the nickel surface during annealing, resulting in an increase in the area of thicker graphene. Therefore, it is obvious that the area of thicker graphene increased at higher annealing temperature (see Fig. S3, ESI†). Due to the increased area of thicker graphene, one can see

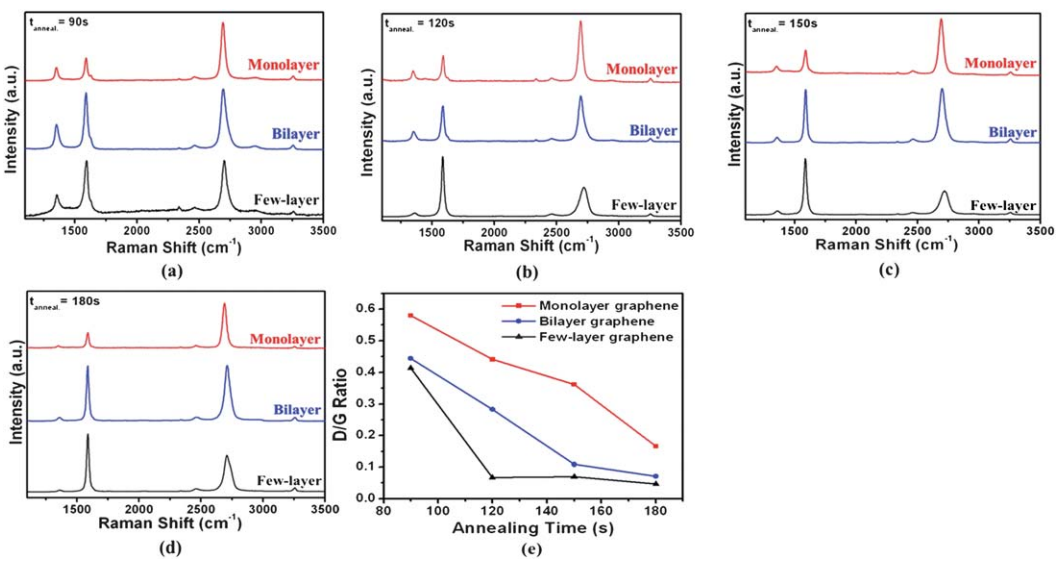

Fig. 4 (a) Raman spectra of mono- to few-layer graphene annealed at 950 °C for 90 s. (b) Raman spectra of mono- to few-layer graphene annealed at 950 °C for 120 s. (c) Raman spectra of mono- to few-layer graphene annealed at 950 °C for 150 s. (d) Raman spectra of mono- to few-layer graphene annealed at 950 °C for 180 s. (e) Ratio of the D to G peak of graphene annealed at various durations.

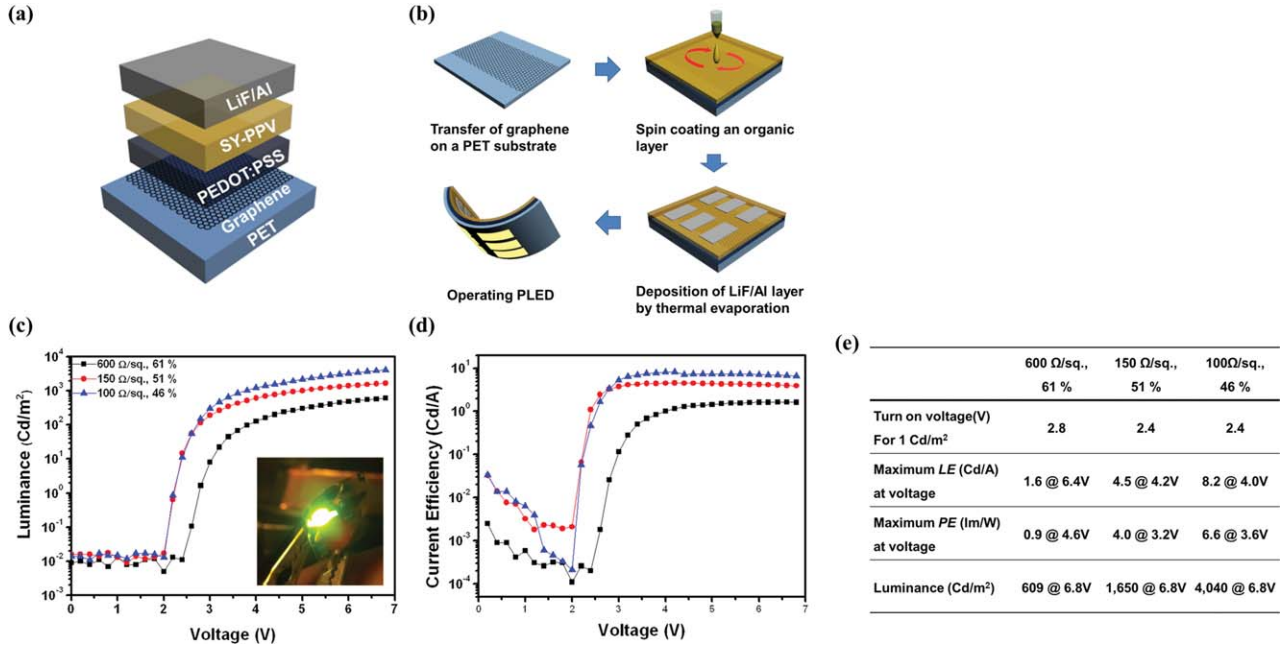

(e)

	600 Ω/sq., 61 %	150 Ω/sq., 51 %	100Ω/sq., 46 %
Turn on voltage(V) For 1 Cd/m²	2.8	2.4	2.4
Maximum *LE* (Cd/A) at voltage	1.6 @ 6.4V	4.5 @ 4.2V	8.2 @ 4.0V
Maximum *PE* (lm/W) at voltage	0.9 @ 4.6V	4.0 @ 3.2V	6.6 @ 3.6V
Luminance (Cd/m²)	609 @ 6.8V	1,650 @ 6.8V	4,040 @ 6.8V

Fig. 6 (a) Device structure of a flexible PLED on the graphene/PET substrate. (b) Schematics of fabrication of a flexible PLED by the solution process. (c) Luminance *vs.* voltage characteristics of flexible PLEDs on graphene with various sheet resistances and transmittances. Inset shows a bent operating PLED. (d) Luminance efficiency *vs.* voltage characteristics of flexible PLEDs on graphene with various sheet resistances and transmittances. (e) Device performance of flexible PLEDs with various sheet resistances and transmittances.

lower sheet resistance and transmittance with higher annealing temperature. To reduce the sheet resistance, the graphene samples were treated with HNO_3. The sheet resistance of HNO_3-treated samples were 2540, 720, 210, and 100 Ω sq.$^{-1}$ at 800, 850, 900, and 950 °C, respectively. There was no significant change in the transmittance. The sheet resistance of the graphene samples was reduced after HNO_3 treatment. It can be ascribed to hole carrier increase due to chemical doping with HNO_3.[3] The sheet resistance and transmittance of the graphene samples were also measured after being transferred onto a PET film. After the growth of graphene, it was transferred onto the PET film by the hot press lamination process. Fig. 3b shows photo images of the graphene samples after transferred onto the PET film. The sheet resistance and the transmittance of graphene samples on the PET film were 250 Ω sq.$^{-1}$ and 64%, respectively.

Graphene was also grown with various durations of annealing. The graphene samples were annealed at 950 °C for 90, 120, 150, and 180 seconds, respectively. Fig. 4 shows the Raman spectra of the graphene samples annealed for various durations (see Table S2, ESI†). According to the known criteria, mono- to few-layer graphene were grown from all samples.

The sheet resistance and the transmittance of the graphene samples annealed for various durations were also investigated. Fig. 5a shows sheet resistance and transmittance of the graphene samples annealed for various durations. The sheet resistance of graphene samples were 1660, 600, 500, and 250 Ω sq.$^{-1}$ for 90, 120, 150 and 180 seconds, respectively. The transmittance of the graphene samples at 550 nm were 84, 82, 75, and 71%, respectively. The sheet resistance and the transmittance decreased with increasing duration of annealing. The amount of carbon diffusing into the nickel increases with time. With increasing duration of annealing, the area of the thicker graphene becomes enlarged and increased (see Fig. S4, ESI†). Consequently, the sheet resistance and the transmittance decreased with longer annealing time. These results were comparable to the ones obtained for graphene grown on the nickel layer using CVD with a gaseous hydrocarbon source (see Fig. S5, ESI†).

The resulting graphene film transferred onto the PET substrate was applied as a flexible and transparent electrode of PLED. The device structure of a flexible PLED fabricated on the graphene/PET substrate consisted of graphene/poly(3,4-ethylenedioxythiophene)poly-(styrenesulfonate) (PEDOT:PSS)/Super Yellow (SY)/LiF/Al as shown in Fig. 6a. The flexible PLED was fabricated by the solution process. Fabrication of the flexible PLED on graphene/PET substrate is schematically described in Fig. 6b. The PEDOT:PSS and SY layers were spin-coated on the graphene/PET substrate and subsequently the LiF and aluminum layers were deposited by thermal evaporation. The device characterizations of PLEDs are presented in terms of the luminance *versus* the applied voltage and the luminance efficiency *versus* the voltage, as shown in Fig. 6c and d. The maximum luminance and luminance efficiency were 4040 Cd m^{-2} at 6.8 V and 8.2 Cd A^{-1} at 4.0 V. The inset in Fig. 6c shows a flexible and yellow-emitting PLED fabricated on the graphene/PET substrate. As summarized in Fig. 6e, among different annealing conditions of graphene, the lowest turn-on voltage and the highest power efficiency were 2.4 V and 6.6 lm W^{-1} at 3.6 V, respectively. To our knowledge, it is the first report on the typical PLED fabricated on the graphene electrode from a solid carbon source although there have been reports on inverted-structure PLEDs,[34] light-emitting electrochemical cells,[35,36] and vacuum deposited organic light emitting diodes.[37] Our demonstration of graphene as a flexible and transparent

electrode of PLED shows that the graphene electrode could be a promising candidate for a flexible and transparent electrode.

Conclusions

In summary, we have demonstrated a simple method for the synthesis of large area and mono- to few-layer graphene on a nickel foil. The CALF was coated on a nickel foil as a solid carbon source. Compared to previous synthesis methods using solid carbon sources, the mentioned carbon source can be easily coated on the large-area metal catalyst layer. The large-area graphene layer could be grown on the nickel catalyst layer due to the uniform thickness of the solid carbon source layer, which was made of the CALF coated by the cold press lamination process. Graphene was grown from the CALF without explosive gaseous carbon sources usually used in the growth of graphene by a CVD method. A series of processes mentioned above could be started and ended with a lamination process and the sheet resistance and transmittance of graphene were controlled by parameters used for the synthesis of graphene. This synthesis method could offer a practical way to synthesize large-area graphene from solid carbon sources. To demonstrate the practical use of graphene, a flexible PLED was fabricated on the graphene electrode synthesized through the method mentioned above. Our demonstration of graphene as a flexible and transparent electrode of PLED shows that the graphene electrode obtained from solid carbon sources could be a promising candidate for a transparent and flexible electrode.

Acknowledgements

This research was supported by WCU (World Class University) program through the National Research Foundation of Korea funded by the Ministry of Education, Science and Technology (R32-10051).

References

1 X. L. Li, G. Y. Zhang, X. D. Bai, X. M. Sun, X. R. Wang, E. Wang and H. J. Dai, *Nat. Nanotechnol.*, 2008, **3**, 538–542.
2 J. Kwon, S. H. Lee, K. H. Park, D. H. Seo, J. Lee, B. S. Kong, K. Kang and S. Jeon, *Small*, 2011, **7**, 864–868.
3 C. Y. Su, A. Y. Lu, Y. P. Xu, F. R. Chen, A. N. Khlobystov and L. J. Li, *ACS Nano*, 2011, **5**, 2332–2339.
4 H. Yamaguchi, G. Eda, C. Mattevi, H. Kim and M. Chhowalla, *ACS Nano*, 2010, **4**, 524–528.
5 X. S. Li, Y. W. Zhu, W. W. Cai, M. Borysiak, B. Y. Han, D. Chen, R. D. Piner, L. Colombo and R. S. Ruoff, *Nano Lett.*, 2009, **9**, 4359–4363.
6 K. S. Kim, Y. Zhao, H. Jang, S. Y. Lee, J. M. Kim, K. S. Kim, J. H. Ahn, P. Kim, J. Y. Choi and B. H. Hong, *Nature*, 2009, **457**, 706–710.
7 Y. Lee, S. Bae, H. Jang, S. Jang, S. E. Zhu, S. H. Sim, Y. I. Song, B. H. Hong and J. H. Ahn, *Nano Lett.*, 2010, **10**, 490–493.
8 Z. G. Wang, Y. F. Chen, P. J. Li, X. Hao, J. B. Liu, R. Huang and Y. R. Li, *ACS Nano*, 2011, **5**, 7149–7154.
9 L. G. De Arco, Y. Zhang, C. W. Schlenker, K. Ryu, M. E. Thompson and C. W. Zhou, *ACS Nano*, 2010, **4**, 2865–2873.
10 Y. Wang, S. W. Tong, X. F. Xu, B. Ozyilmaz and K. P. Loh, *Adv. Mater.*, 2011, **23**, 1514–1518.
11 S. Bae, H. Kim, Y. Lee, X. F. Xu, J. S. Park, Y. Zheng, J. Balakrishnan, T. Lei, H. R. Kim, Y. I. Song, Y. J. Kim, K. S. Kim, B. Ozyilmaz, J. H. Ahn, B. H. Hong and S. Iijima, *Nat. Nanotechnol.*, 2010, **5**, 574–578.
12 W. H. Lee, J. Park, S. H. Sim, S. B. Jo, K. S. Kim, B. H. Hong and K. Cho, *Adv. Mater.*, 2011, **23**, 1752–1756.
13 K. S. Novoselov, A. K. Geim, S. V. Morozov, D. Jiang, Y. Zhang, S. V. Dubonos, I. V. Grigorieva and A. Firsov, *Science*, 2004, **306**, 666–669.
14 H. Huang, W. Chen, S. Chen and A. T. S. Wee, *ACS Nano*, 2008, **2**, 2513–2518.
15 P. W. Sutter, J. I. Flege and E. A. Sutter, *Nat. Mater.*, 2008, **7**, 406–411.
16 N. Liu, L. Fu, B. Y. Dai, K. Yan, X. Liu, R. Q. Zhao, Y. F. Zhang and Z. F. Liu, *Nano Lett.*, 2011, **11**, 297–303.
17 J. A. Rodriguez-Manzo, C. Pham-Huu and F. Banhart, *ACS Nano*, 2011, **5**, 1529–1534.
18 A. J. Pollard, R. R. Nair, S. N. Sabki, C. R. Staddon, L. M. A. Perdigao, C. H. Hsu, J. M. Garfitt, S. Gangopadhyay, H. F. Gleeson, A. K. Geim and P. H. Beton, *J. Phys. Chem. C*, 2009, **113**, 16565–16567.
19 M. Zheng, K. Takei, B. Hsia, H. Fang, X. B. Zhang, N. Ferralis, H. Ko, Y. L. Chueh, Y. G. Zhang, R. Maboudian and A. Javey, *Appl. Phys. Lett.*, 2010, **96**, 063110.
20 C. Orofeo, H. Ago, B. S. Hu and M. Tsuji, *Nano Res.*, 2011, **4**, 531–540.
21 L. Baraton, Z. B. He, C. S. Lee, J. L. Maurice, C. S. Cojocaru, A. F. Gourgues-Lorenzon, Y. H. Lee and D. Pribat, *Nanotechnology*, 2011, **22**, 085601.
22 L. M. A. Perdigao, S. N. Sabki, J. M. Garfitt, P. Capiod and P. H. Beton, *J. Phys. Chem. C*, 2011, **115**, 7472–7476.
23 M. S. Xu, D. Fujita, K. Sagisaka, E. Watanabe and N. Hanagata, *ACS Nano*, 2011, **5**, 1522–1528.
24 Z. Z. Sun, Z. Yan, J. Yao, E. Beitler, Y. Zhu and J. M. Tour, *Nature*, 2010, **468**, 549–552.
25 H. Ago, I. Tanaka, C. M. Orofeo, M. Tsuji and K. Ikeda, *Small*, 2010, **6**, 1226–1233.
26 S. J. Byun, H. Lim, G. Y. Shin, T. H. Han, S. H. Oh, J. H. Ahn, H. C. Choi and T. W. Lee, *J. Phys. Chem. Lett.*, 2011, **2**, 493–497.
27 Z. W. Peng, Z. Yan, Z. Z. Sun and J. M. Tour, *ACS Nano*, 2011, **5**, 8241–8247.
28 G. D. Ruan, Z. Z. Sun, Z. W. Peng and J. M. Tour, *ACS Nano*, 2011, **5**, 7601–7607.
29 A. C. Ferrari, J. C. Meyer, V. Scardaci, C. Casiraghi, M. Lazzeri, F. Mauri, S. Piscanec, D. Jiang, K. S. Novoselov, S. Roth and A. K. Geim, *Phys. Rev. Lett.*, 2006, **97**, 187401.
30 X. S. Li, W. W. Cai, J. H. An, S. Kim, J. Nah, D. X. Yang, R. Piner, A. Velamakanni, I. Jung, E. Tutuc, S. K. Banerjee, L. Colombo and R. S. Ruoff, *Science*, 2009, **324**, 1312–1314.
31 S. S. Chen, W. W. Cai, R. D. Piner, J. W. Suk, Y. P. Wu, Y. J. Ren, J. Y. Kang and R. S. Ruoff, *Nano Lett.*, 2011, **11**, 3519–3525.
32 W. Wu, L. A. Jauregui, Z. H. Su, Z. H. Liu, J. M. Bao, Y. P. Chen and Q. K. Yu, *Adv. Mater.*, 2011, **23**, 4898–4903.
33 D. A. Porter and K. E. Easterling, *Phase Transformations in Metals and Alloys*, 2ndedn, 2004, pp. 63–68.
34 J. O. Hwang, J. S. Park, D. S. Choi, J. Y. Kim, S. H. Lee, K. E. Lee, Y. H. Kim, M. H. Song, S. Yoo and S. O. Kim, *ACS Nano*, 2012, **6**, 159–167.
35 P. Matyba, H. Yamaguchi, G. Eda, M. Chhowalla, L. Edman and N. D. Robinson, *ACS Nano*, 2010, **4**, 637–642.
36 P. Matyba, H. Yamaguchi, M. Chhowalla, N. D. Robinson and L. Edman, *ACS Nano*, 2011, **5**, 574–580.
37 T. H. Han, Y. Lee, M. R. Choi, S. H. Woo, S. H. Bae, B. H. Hong, J. H. Ahn and T. W. Lee, *Nat. Photonics*, 2012, **6**, 105–110.